

TWO-DIMENSIONAL ELECTRIC IMAGING: A NON-INVASIVE TOOL FOR HELPING HYDROGEOLOGICAL AND GEOTECHNICAL PROBLEMS IN URBAN AREAS

Jorge L. Abril Benjumea ^{*}, Olivar A. L. de Lima and Luiz E. Campos

ABSTRACT. Two-dimensional electrical images of resistivity and time-domain induced polarization (IP) in conjunction with standard penetration tests (SPTs) were used to investigate the subsurface drainage patterns and the stability of underground geological structures in two endangered earth-sloping areas, referred as LEM (Luiz Eduardo Magalhães) and LVF (Luiz Viana Filho). They are located along new streets cutting across hill slopes with thick clayed and silt-sand weathering products, which are potentially susceptible to water seepages and landslides. The Schlumberger electrode array was used to obtain well-controlled geo-electrical soundings for two geophysical traverses extending across the unstable zone in the LEM damaged area. A dipole-dipole array was used to survey three geo-electrical traverses extending across the water-seeping LVF area. The constructed pseudosections of apparent resistivity and chargeability were automatically inverted using the RES2DINV package, controlled by SPT and lithological data from samples collected by drilling through the regolith layers. The results of geological and geotechnical data allowed identifying in the LEM study area failure conditions, weathering of geological material and high slopes that contributed to the landslide reported on LEM Avenue. Additionally, the results of the LVF Avenue identified a rainwater infiltration in the central garden in front of the buildings of this residential area.

Keywords: inverse problem, dipole-dipole survey, induced polarization, geotechnical engineering, hydrogeology.

RESUMO. Imagens bidimensionais de resistividade elétrica e polarização induzida em conjunto com ensaios de penetração padrão (SPT) foram empregados na avaliação da geologia de subsuperfície em duas áreas referidas como LEM (Luiz Eduardo Magalhães) e LVF (Luiz Viana Filho), as quais situam-se em avenidas que cortam estruturas de encostas e vertentes de colinas, constituídas de materiais argilosos e silico-arenosos, com alto grau de meteorização, os quais são potencialmente susceptíveis a escorregamentos. O arranjo de eletrodos Schlumberger foi usado para obter sondagens elétricas em dois transectos sob a área afetada em LEM. Três perfis, utilizando o arranjo Dipolo-Dipolo, foram levantados ao longo da área LVF. As pseudo-seções de resistividade aparente e cargabilidade foram invertidas usando o software comercial RES2DINV, controladas por dados de SPT e informação litológica de amostras do solo perfurado em todo o regolito. Os resultados dos dados geológicos e geotécnicos permitiram identificar na área de estudo LEM condições de falhamento, meteorização de material geológico e altas pendentes que contribuíram no escorregamento reportado na Avenida LEM. Além disso, os resultados da área LVF identificaram uma frente de infiltração de água de chuva na área do jardim central na frente dos edifícios desta área residencial.

Palavras-chave: problema inverso, arranjo Dipolo-dipolo, polarização induzida, engenharia geotécnica, hidrogeologia.

INTRODUCTION

One challenge for geotechnical engineering in Salvador city, Bahia State, Brazil, involves the topographic relief and the presence of a thick weathered layer covering its urban areas. The following factors are relevant to geotechnical problems beyond the environmental conditions: (i) a disordered urban growth leading to inappropriate areas being occupied by poor populations; (ii) an urban expansion project to increase the city road network by constructing large and sometimes inadequate or ill-dimensioned avenues, along natural water drainage valleys. During rainstorm autumn-winter periods, the lowest zones throughout the city flood, mud and soil slide along embankments and slopes causing the loss of countless lives and severe damage to the state economy.

Globally, geophysics has been used for geotechnical investigations for several years. Geoelectrical and electromagnetic methods, in particular, have successfully investigated soil and stability conditions, that cause many civil engineering problems (Bogoslovsky and Ogilvy, 1977; Godio and Bottino, 2001). Characterizing and determining the strength of underground soil are the basic requirements for designing the foundation of important civil engineering buildings. Several attempts to integrate geo-electrical characterizations and geotechnical data have been made (Cosenza et al., 2006; Friedel et al., 2006; Sudha et al., 2009). Samouëlian et al. (2005) have reviewed the use of electrical methods for soil determination and slope instability.

In this paper, two geophysical and geotechnical experiments are discussed for investigating the drainage and soil mechanics beneath the urban area of Salvador. The first area is located along the LEM (Luiz Eduardo Magalhães) Avenue, an important route constructed to improve vehicle flux within the city. In 2005, a large landslide occurred in a slope of this avenue and required almost one year to stabilize and recompose the structural damage. The second area is located in a middle class residential expansion area on LVF (Luiz Viana Filho) Avenue and is related to intermittent water

filtration outflows along an artificial slopping cut near a large apartment building. These two areas are shown in Figure 1.

The equipment used in these investigations was a SYSCAL R2 system from Iris Instruments (France). The soundings were performed using a 2s pulse duration, with preset time values for the IP sampling windows. Inversion of the electrical data was carried out using a cell-based inversion technique exploited by the RES2DINV code, as described by Loke and Barker (1996) and by Geotomo (2010). This technique subdivides the underground model into a number of rectangular cells, whose positions and sizes uses a default pattern, or can be specified by the interpreter. The inversion is based on a regularized optimization, which uses either a smooth least squared (L2-norm) or a robust blocky (L1-norm) minimization approach. The (L2 norm) regularization approach is based on calculating solutions with a low contrast of a certain physical property. In contrast, there is the (L1 norm) regularization approach, that favors more blocky structures in a similar way to minimize the high contrast associated with a determined physical property (Rudin et al., 1992).

By a consistence analysis, the inverted sections presented for the LEM and LVF areas were obtained using the second option.

These studies aimed to develop efficient procedures to adequately image the subsurface geology for hazardous areas posing a real and potential risk for landslides. The final results were expressed as the composition and internal soil horizon structures, water table configurations, substratum topographies and both clay and water saturation distribution along their subsurface. These results were useful to design engineering structures to drain and contain the earth materials along these dangerous areas.

GEOLOGICAL SETTING

The geological substratum in most of Salvador city consists of high-grade metamorphic rocks of Pre-Cambrian age, including gneisses and migmatites, with a pervasive foliation oriented NNE, as described in Barbosa et al. (2005). This hard-rock

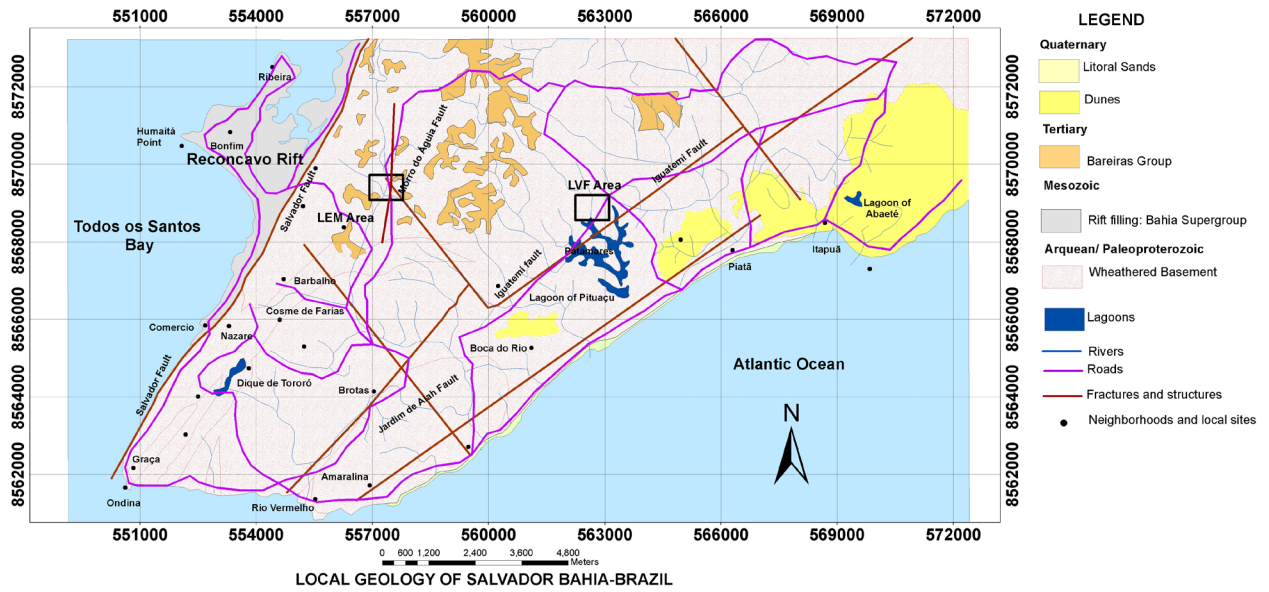


Figure 1 - Maps of Salvador city with reference to the country, state and Recôncavo rift basin.

terrain is part of the structural unit Salvador High, and corresponds to the oriental limit of the Mesozoic Recôncavo sedimentary rift-basin (Fig. 1). The city grew partly over this structural high and partly over the sedimentary basin. Both units experience successive tectonic episodes of brittle failure, with the Salvador Fault being the most impressive faulted controlled zone – extending over 100 km, with over 6.0 km of total vertical displacement. They are also affected by other minor faults and dense conjugated fracturing oriented N30-40E, E-W and N30-40W. Other recognized faults in the area are the Iguatemi and Morro do Águia faults, the former was identified during this work (Fig. 1). Such old structural features, reactivated when the Recôncavo rift formed and afterwards, appear as large lineaments in aerial photos and satellite images of the city, and control the surface water drainage in the area (de Moraes, 2008). The densely fractured metamorphic rocks experience deep chemical and physical weathering and debris transport processes during the tropical rainy conditions, which undulate the surface morphology into gently hills and valleys covered by thick weathered soil horizons. This regolith is very thick (over 20 m in thickness) with the following characteristic horizons: (i) A thin washed-sand layer, predominantly containing quartz and decomposing organic matter; (ii) A masked red to

brown silt-sand horizon, where most of the original mineral assemblage was replaced and only the resistant ones (quartz, micas, garnet and zircon) remain. A ferruginous concretionary lateritic layer may develop in this zone; (iii) A partially altered horizon containing decomposed material, where the original texture and some structures still exist, that contains more resistant portions of the gneissic rocks.

THE LEM EXPERIMENT

The rainfall-induced landslide on LEM Avenue occurred on the 27th of August 2005, after a severe six-month rainy period in Salvador. The photo in Figure 2 shows that the wedge-shaped sliding block was bounded by a curved rupture surface, extending across one side of the road. The underground compression of the decomposed material uplifted the asphalt in one track of the road over 3.0 m height mound. Along several fractured surfaces within the sliding block, the altered material exhibits strong shearing, milonitization and an abundance of graphitic slicken-slides material. These are the main evidences to recognize the Morro do Águia fault damage zone crossing through the area, which partially control the sliding.

The photo of Figure 2 also depicts the layout of geotechnical drill hole locations and the disposition of the two geophysical cross-sections,

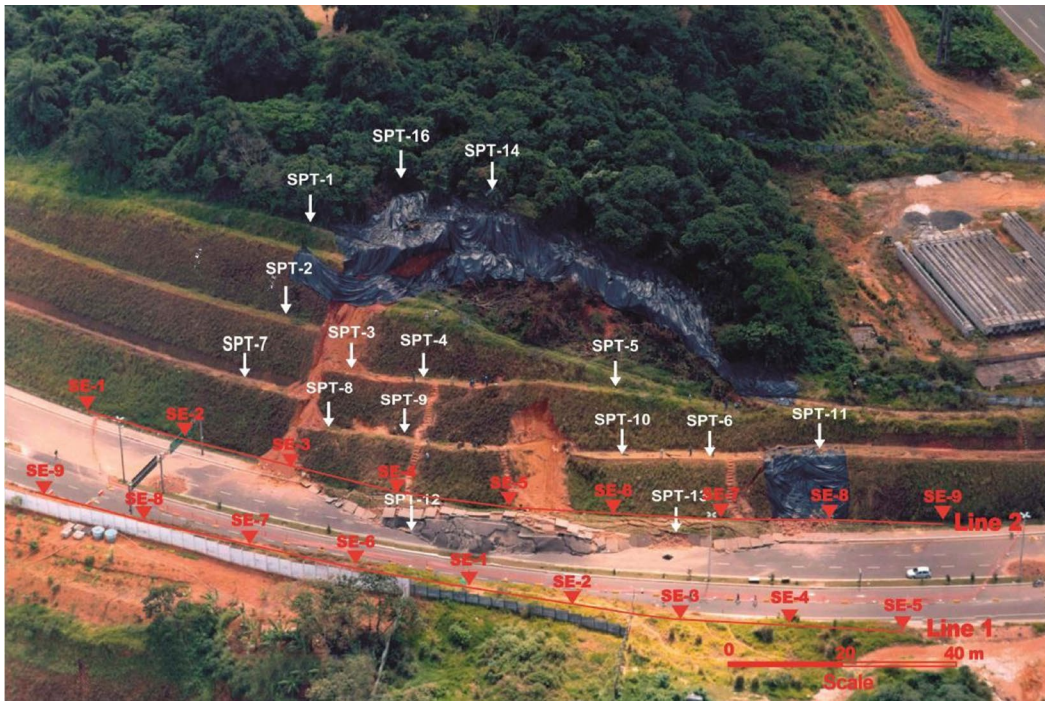


Figure 2 - Photo of the LEM Avenue landslide showing the geophysical and geotechnical layout. Adapted from (Benjumea, 2018).

composed by spaced Schlumberger electrical soundings centered at the indicated positions, and also the approximated location of the referred water exploration well.

Geotechnical Results

Geotechnical testing comprising standard penetration percussion-drillings and detailed soil samples analysis were performed at 19 sites selected throughout the affected area. Figure 3a is a cross-sectional view of the road showing the following features: (i) the original hill slope surface; (ii) the cut surface allowing the road passage; and (iii) the topographic surface after the sliding event. Overlaying data from four SPT drill holes over this figure reveals a lithological zonation and the mechanical soil layer consistency to a depth of 20 m.

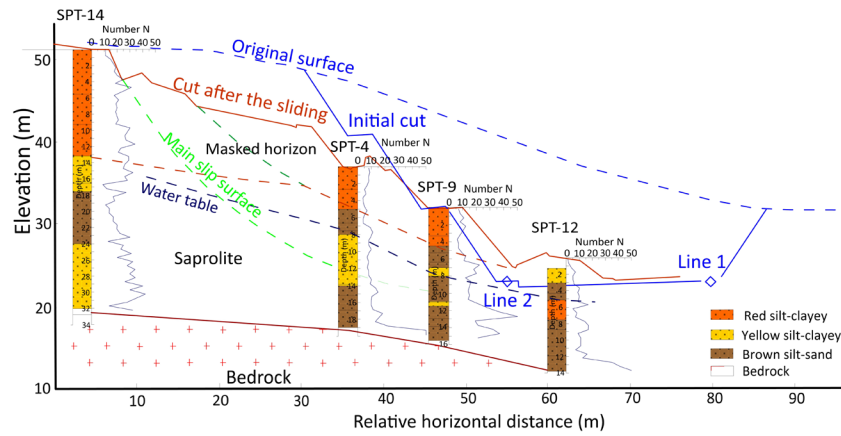
The SPT-14 well was located on a hilltop and closely reflects the original consistency of the non-disrupted, weathered layer. The soil strength was characterized by the number of blows (N) per 25 cm of penetration, which was normally above 20. The other three wells were located inside the sliding zone and exhibited a smaller cohesion, with an N below 10. In addition to providing these samples, the boreholes were also used to measure the groundwater level as depicted in Figure 3a. Figure 3 also shows the position of the

geo-electrical survey lines and outlines the main surface rupture and another internal surface involved in the sliding event. The SPT-12 and SPT-13 were located in Figure 3b near to Line 2 of the LEM, depicted in Figure 2, with the goal of finding a good correlation between the geophysical data and the direct information extracted from the subsoil.

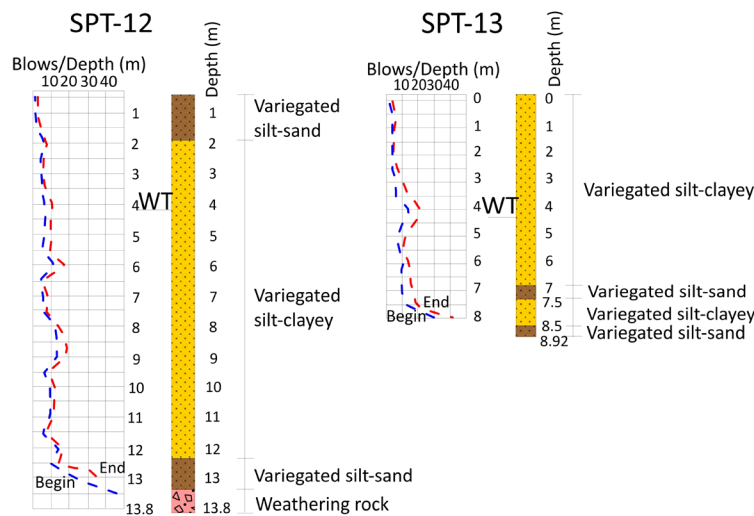
Geophysical Results

Two-dimensional electrical images of the resistivity and induced polarization were used to map the underground subsurface regolith layers and to determine the bedrock depth in the area. The survey was performed in September / 2005 and consisted of 18 Schlumberger electrical soundings along two parallel lines at the margins of the double-lane road. One extended over its affected side and another over the opposite side, indicated as lines 2 and 1, respectively, in the cross-section of Figure 3. The sounding centers were 20 m apart, and the maximum AB/2 spacing used for each expansion was 100 m. Each profile was 180 m long.

Due to low cost and easy geophysical acquisition, it was used the geo-electrical sections of VES in the LEM area, which allowed a good identification of sharp boundaries and vertical resolution.



(a) - Geological, geotechnical and hydrogeological information of LEM area



(b) - Drilling holes of SPT surveyed near to Line 2 in LEM area

Figure 3 - Geological, hydrological and geotechnical cross-sections and two drill holes for the main LEM sliding surface features before and after the accident. Adapted from Benjumea (2018).

The suitability of the inversion results were evaluated by the use of the mean absolute error between the measured and the computed apparent resistivity and chargeability values, for the number of points in each section. The inverted resistivity and IP models obtained in the area are shown in Figures 4 to 7 for lines 1 and 2, respectively.

The resistivity and IP distributions within the subsurface soil below line 1, which was less affected by the landslide (Figs. 4 and 5), exhibited large lateral variations in the upper soil materials. The high ρ_a and low m_a values in the upper zone, suggest it was highly porous and low water content in the central part. The water table depth varied from 6 to 9m, along the profile. The large IP values in the soil layer and basement block between soundings SE-7 to SE-9, should be related to the

dispersed graphite and other conductive minerals, which are strong sources for IP effects. A sub-vertical zone with intermediate resistivity and high IP values, between soundings SE-6 to SE-4, was related to the sheared damage zone in the Morro do Águia fault, and its densely fractured materials. In addition, it is observed a vertical structure of moderate resistivity and high IP values between soundings SE-7 to SE-6, also associated with the Morro do Águia fault.

The resistivity increase and chargeability reduction observed in the top layer, between soundings SE-4 and SE-6, were a result from the combined influence of topography and lateral electrical heterogeneities within the bulge created by the landslide. The absolute errors for this line, after six iterations, were of 10.9% and 1.7% for the concurrent resistivity and IP inversion.

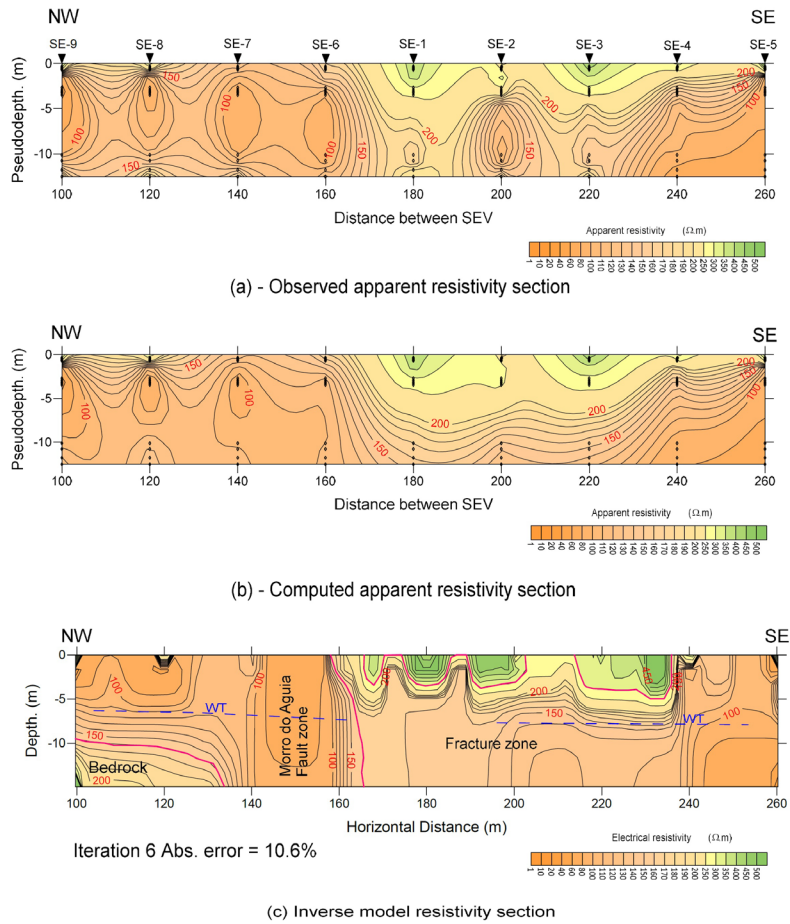


Figure 4 - Resistivity distribution along line 1 and the interpreted geo-electrical model.

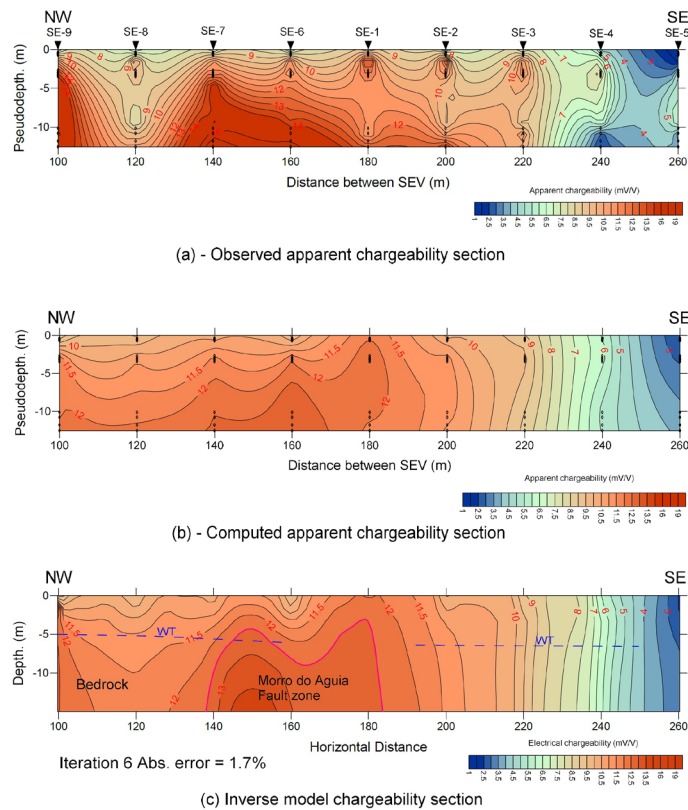


Figure 5 - Chargeability distribution along line 1 and the interpreted geo-electrical model.

Figures 6 and 7 show the pseudo-sections and the electrical-depth models for line 2 crossing through the uplifted side of the road. Both the resistivity and IP true images exhibited strong electrical contrast in the most superficial part of the weathered material. Such contrast was marked by a sharp resistivity transition above 600 Ω .m (green) to 60 Ω .m (orange). The IP effect was also strong within this upper layer. For this line the absolute errors, after five iterations, were of 8.8% and 1.3%, respectively.

The high resistivity and chargeability of the regolith, between soundings SE-1 and SE-5, suggest a porous material with a reduced clay content (a sand-silt layer) and low water saturation. The east side of the fault trace is rich in clay with high water content. The main slip mass was concentrated within this superficial dewatered soil material after sliding.

Beneath this variable soil covering the crystalline, partially altered rocks (below 9 m depth) were determined by several sub-vertical electrical structures. The most notable was located in the central-eastern portion, between soundings SE-5 and SE-9. It has low resistivity values and moderate chargeability and contained the most sheared portion of the Morro do Águia fault zone. There was a wide transitional zone with intermediate resistivity, considered to be a thick permeable portion of the fractured basement unit.

THE LVF EXPERIMENT

A geotechnical problem during the construction of two apartment buildings near LVF Avenue involved several points of continuous water seepage of unknown origin from a lateral cut in the west side of the hill, where the buildings were supported. Two possibilities were discussed: one quoted the existence of pipeline leaks in the network supplying water for the neighbor condominium; the other assumed a vertical infiltration from rainwater spread by the lateral subsurface as an unsaturated downward flow above the water table surface.

Given that this infiltration may cause slippage and local instabilities within the sloped terrain, cement was injected into boreholes opened in the side of Ibiassucê Street, as shown in Figure 8, to

stabilize the weathered soil cover and control the water seepages. Furthermore, sub-horizontal drains were installed into the cemented hill slope.

Despite these stabilization procedures, the exudation of water from both the soil nailing cut and the adjacent western slope remained persistent, even during a period with no rainfall in July and August, 2012. A detailed geophysical work was considered to clarify this geotechnical problem, to determine the underground drainage pattern and to provide useful physical information to define a hydrological solution.

Geotechnical Result

The topographic map in Figure 8 shows some fracture lineaments identified by deep grooves in satellite images from Google Earth and through direct observation on lateral road cuts accessing the area.

Geotechnical percussion drill holes were used to identify four horizons of different litho-mechanical constitutions within the area. The geological cross-section in Figure 9, constructed based on five SPTs, show the vertical distribution of these units, which were characterized as follows: (i) the upper layer, dominant in the western area, based on its composition and low cohesion was identified as a cut and fill soil layer created during the road construction; (ii) a masked leached horizon rich in quartz and other resistant minerals, which exhibited a medium to moderate mechanical cohesion; (iii) a saprolitic horizon of altered rock with some textural and compositional elements preserved from the original altered rocks, and usually characterized by high cohesion; and (iv) the fresh or slightly altered rock zone, which was virtually impenetrable to percussion.

Figure 9 also shows the underground configuration of the water table depth within the central Ibiassucê Street garden. The saturated flow proceeded from west to east along the main building fronts. The topographic descent in the embankment obscured the infiltration and sub-saturated flow occurrence within the vadose zone of the aquifer. Inside the buildings the surface and subsurface runoffs were oriented approximately northeast, along the surface drainage course (Fig. 8).

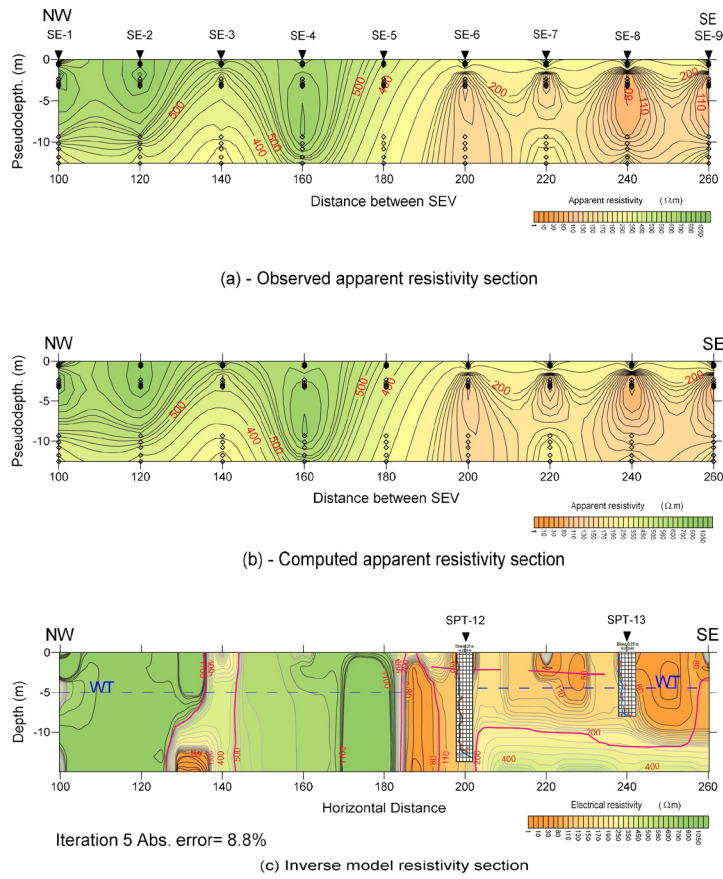


Figure 6 - Resistivity distribution along line 2 and the interpreted geo-electrical model.

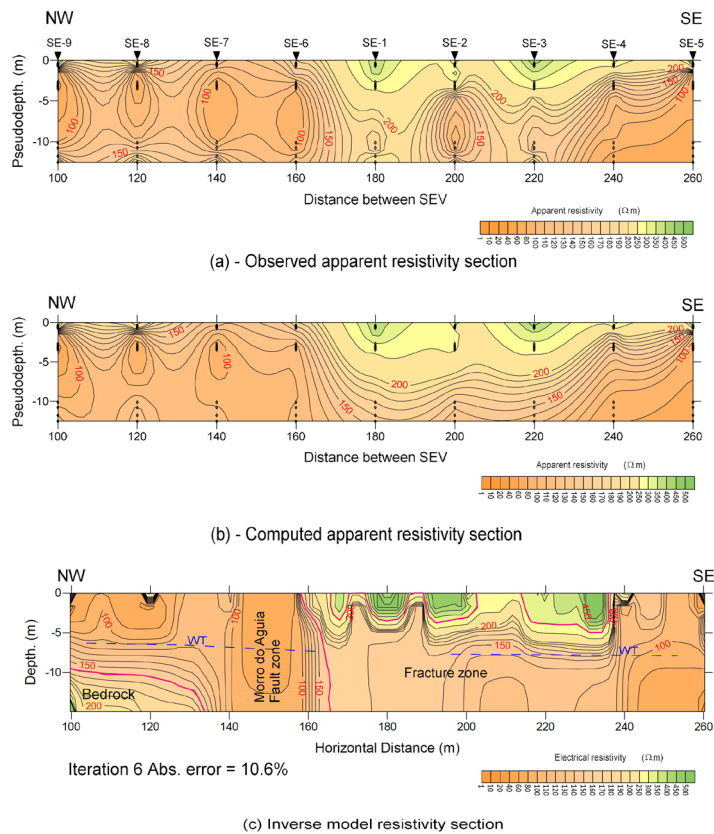


Figure 7 - Chargeability distribution along line 2 and the interpreted geo-electrical model.

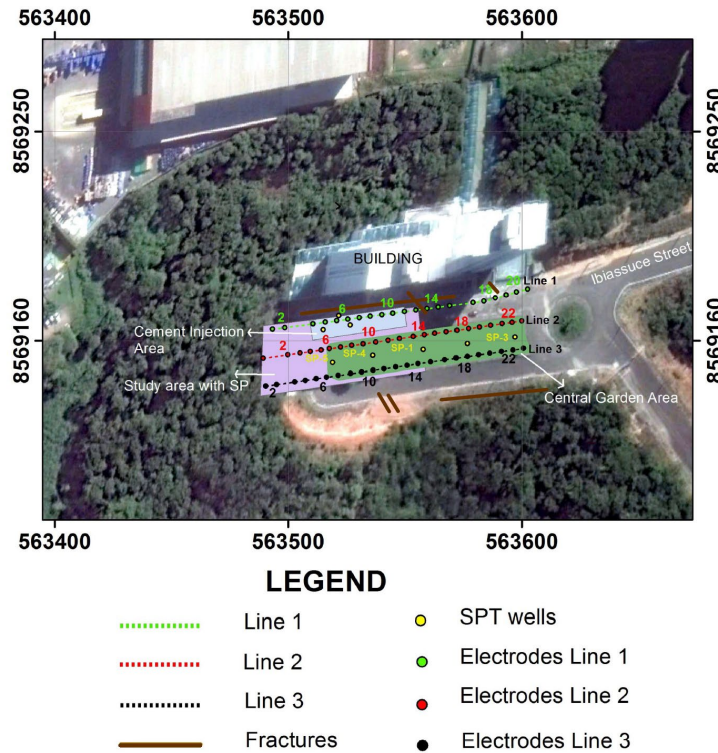


Figure 8 - Building data and survey line layout on a Google image of the LVF area having hydrologic and geotechnical problems.

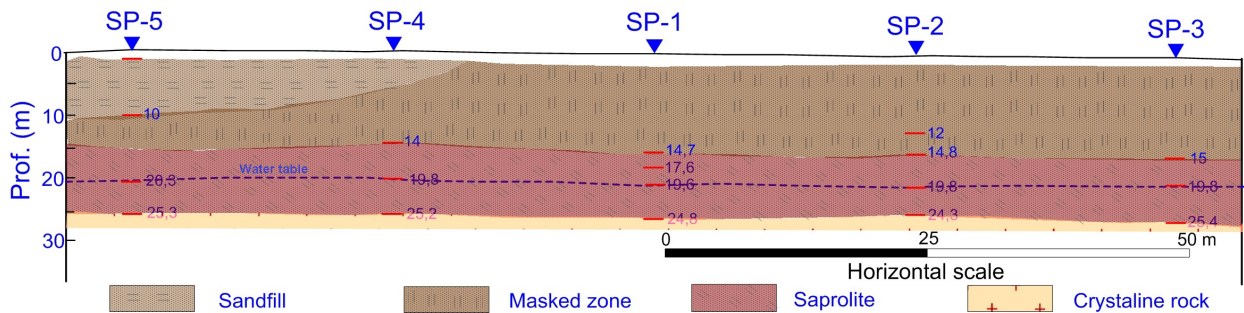


Figure 9 - Geologic and geotechnical cross-section along the LVF area showing the weathered horizon zonation.

Geophysical Results

The hydrodynamic goals defined above were achieved via geo-electrical methods using a multi-profiling technique, measuring simultaneously the electrical resistivity and the time-domain induced polarization of the subsurface geology. Three geo-electrical cross-sections were surveyed along the blue lines shown in Figure 8.

The 2-D imaging provided the underground geological structure, the lithological soil horizon composition and the petrophysical characteristics (porosity and water saturation), as well as the tracking of the more permeable portions, down to a depth of 15 m. The apparent resistivity and apparent chargeability pseudo-sections were constructed from measurements made with the dipole-dipole electrode arrays, using a basic

electrode separation of 5 m and 8 levels of investigations, designed to explore the subsurface up to the desired depth.

All electrode positions over the asphalted road were opened up to the top of the soil layer using a portable rotary drilling machine and a six-inch diameter bit. In the central garden, the roles were made using an auger of the same diameter. Stainless steel rods firmly fixed to the ground were used as current electrodes, and the holes were filled with salt water. Porous pots, with a central copper wire spirals immersed in super-saturated copper sulfate solutions, were used as the potential measuring electrodes.

Figures 10 through 12 show the results from the three geo-electrical cross-sections detailing the subsurface hydrology around the main exudation

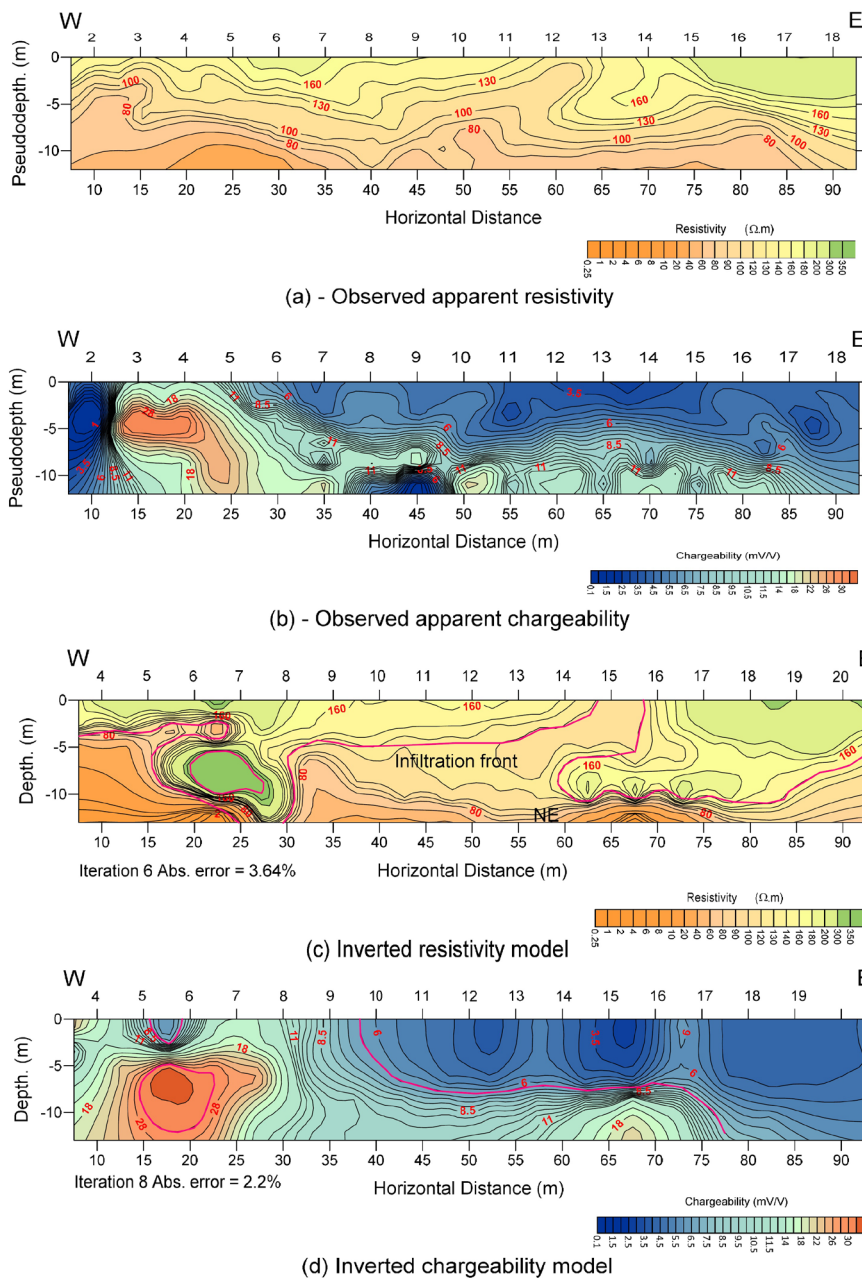


Figure 10 - Resistivity and chargeability distribution along line 1 (LVF area) and the interpreted geo-electrical models.

area. These figures contain the observed and computed apparent resistivity and chargeability data, and the two inverted models for the true resistivity and chargeability of the subsurface geology. To unify the analysis, it was used the same ranges of values representing resistivity and chargeability data.

This survey also required solving two interesting problems. The first was to optimize the voltage between current electrodes, for $n = 1$ to 8, in order to assure a good signal-to-noise ratio, even at the farthest potential electrode pairs.

Repeated reading at certain stations with different input voltages resolved this issue. The second problem was related to negative apparent resistivity measurements obtained at 15 specific stations. The negative values are real, as confirmed by field acquisitions using reciprocity principle, through interchanging the roles of current and potential electrode pairs. In addition, recent literature on two-dimensional geo-electrical simulations has shown that some special geological structures, either U-shaped conductive model or buried metal structures beneath the

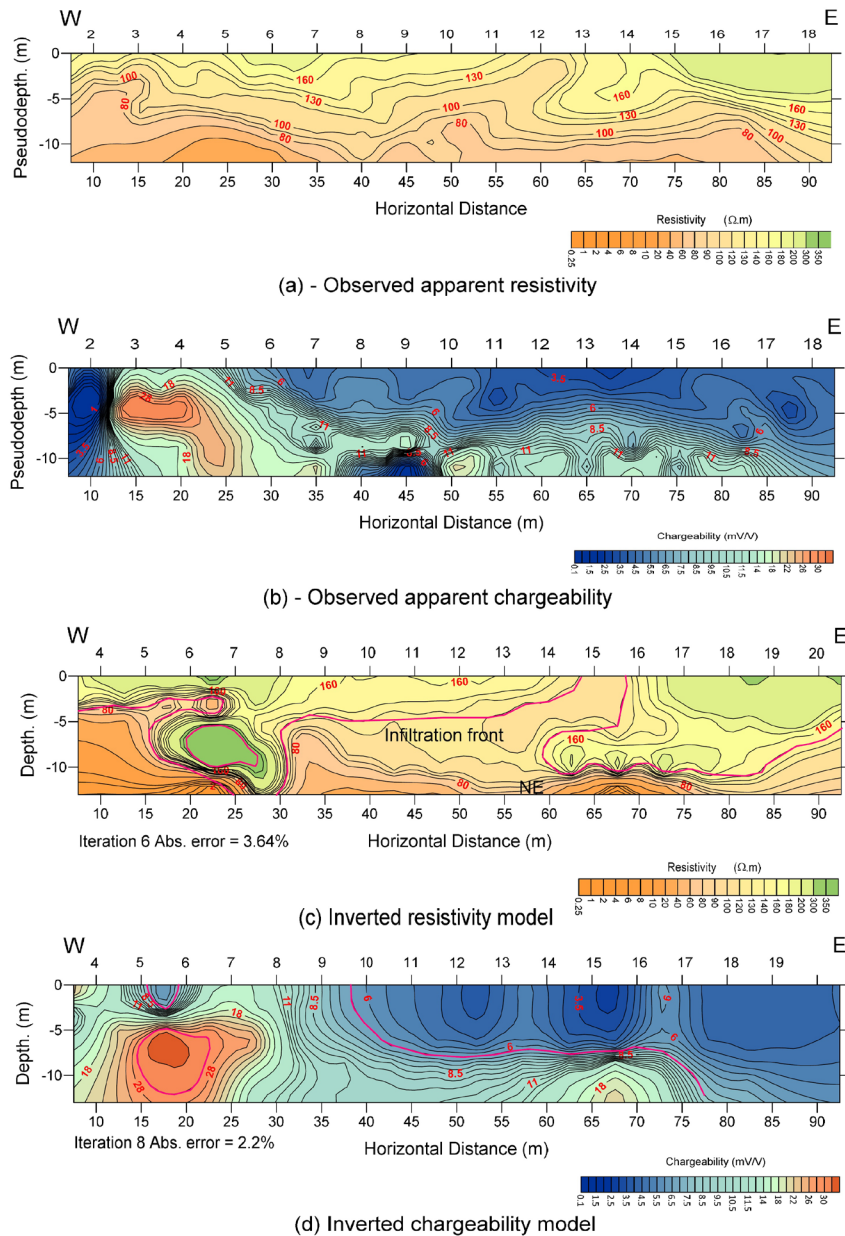


Figure 11 - Resistivity and chargeability distribution along line 2 (LVF area) and the interpreted geo-electrical models.

surface, can, in fact, produce negative apparent resistivity values (Jung et al., 2009; Oh et al., 2011). In the study case, negative values for line 1, in which all electrodes were positioned in holes crossing the asphaltic layer (see Fig. 8 for location), could be strongly influenced by the soil-cemented zone in the western part of this section.

However, the RES2DINV package does not provide an explicit option to work with negative ρ_a values. In this sense, to avoid the effect of such negative points, it was used the robust data constrain (L_1 norm) included in the software. This option causes the reduction of the absolute difference between measured and calculated

apparent resistivity values, allowing all negative values of line 1 to be omitted in the input data file, without affecting inversion results. All these operations are performed automatically in the RES2DINV program.

The statistical results were within an acceptable range (an absolute median error of 18.4%, after seven iterations) and the inverted electrical images were consistent with the two other sections.

Solved the negative resistivity question, it was discussed the inverted results of 2-D electrical images obtained with the RES2DINV package, which produced the final inverted resistivity and chargeability models shown in Figures 10c and 10d.

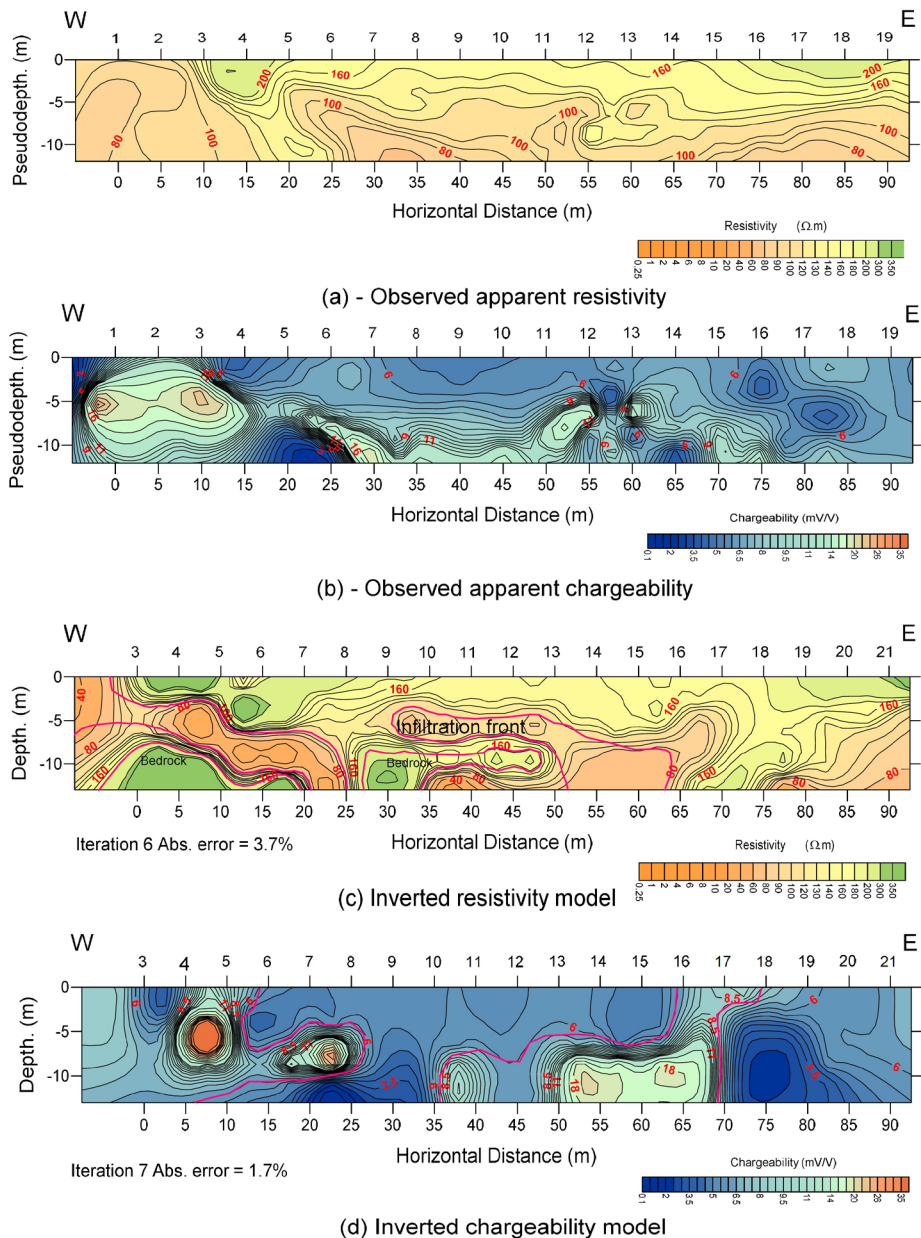


Figure 12 - Resistivity and chargeability distribution along line 3 (LVF area) and the interpreted geo-electrical models.

The resistivity model (Fig. 10c) suggests that the altered materials down to a 3.5 m depth exhibited a moderate resistivity (above 150 $\Omega.m$). The blocks marked as A and B have true resistivity well above 800 $\Omega.m$, and show low to moderated IP effect. They are certainly related to the large amount of cement injected for draping the regolith below the indicated area in Figure 8, and also in the underground supporting structure for the buildings.

The boundary of blocks A and B appears to be controlled by intersecting fracture sets within the altered material. Below and to the

sides of the lower resistive block B, there is the development of an intermediate resistive zone (resistivity between 5 and 60 $\Omega.m$), indicating a porous material with water content higher than the layer directly above it. The more resistive portions of this material, normally with high IP effect, may indicate the most permeable zones, where the rainwater saturation progress faster. Below this layer of intermediate resistivity, there is an important portion of fractured rock that displays resistivity over 800 $\Omega.m$ and intermediate chargeability values indicating the existence of clay minerals and permeable materials of moderate water content.

The chargeability model (Fig.10d) shows high values (> 30 mV/V) in the western portion, which correspond to the conducting zone described above, and supports a higher porosity and water content above and to the west of the cemented block. Several shallow areas (up to 6.0 m deep) with high chargeabilities seem to indicate the presence of buried metals used in the building infrastructure.

Figures 11 and 12 show the results for lines 2 and 3, respectively, which are 12.8 m and 25.6 m south of line 1. Only three electrodes were positioned in the asphalt holes at the end of the area (Fig. 8). No negative apparent resistivity values were registered along these two lines. The inversion yielded a 4.2% absolute median error in resistivity, after six iterations.

The final resistivity model for line 2 identified the following elements: (i) an upper layer with low saturation and resistivity above 120 Ω .m, with lateral variations observed mainly in the central part of the profile; (ii) a conducting interval over 5.0 m thick that sloped from east to west, and associated with a higher degree of saturation (infiltration front). This area seemed to grow from east to west, with a ring of almost complete saturation in the western section; (iii) the conductive capillary fringe zone was practically leveled below 12.5 m; (iv) one highly resistive block of limited lateral extent, located between stations 6 and 7, appears as resulting from the lateral influence caused by the underground cementation zone. The IP data more tenuously reflect the variation in saturation with depth and its increase in the western part of the profile. The statistical fittings were of absolute mean errors of 3.64% and 2.2%, for the concurrent resistivity and IP inversion after six iterations.

For line 3 (Fig. 12), the adjusted electrical models indicated a persistent conductive and chargeable sub-horizontal layer between depths of 5 and 11m. This layer was sandwiched between more resistive and less chargeable horizons, which suggest a rainwater infiltration front, advancing downward to

recharge the crystalline aquifer. Remarkably this front is slightly deeper in the western section, which suggests rapid progress along a more permeable belt in the regolith. The western portion of the section has a lower resistivity and high IP, suggesting a large increase in water content and a faster progress of flow along a permeable zone inside the regolith. Yet the lateral effects caused by the cemented block were notable. The statistical fits for these results also yielded absolute median errors of 3.7% and 1.7%, after six concurrent iterations.

Thus, the high resistivity and moderate IP layers in all three sections (except for blocks A to B) represent the most permeable and washed portion of the regolith in the area. The intermediate resistive zones represent the silt-sand portion of the altered material, having yet high water contents (an advancing infiltration front). The most conductive horizons are quite argillaceous (in general with low IP) and less permeable subsurface paths, retarding the aquifer recharge.

CONCLUSIONS

The LEM geophysical work indicates the 2005 landslide was favored by the natural geological conditions of a hill slope crossed by a geological fault, having a deep weathering cover. These natural conditions were altered by the artificial cuts made to construct the avenue, and two additional triggering events: the strong rains in Salvador during the months prior to the accident and an oriented suction from groundwater withdrawn by a nearby pumping well.

The geophysical results obtained from the LVF experiments supported that the filtration through the hillside cut on the west boundary of the building resulted from the widespread drainage and infiltration of rainwater centered in the central garden in front of the buildings. The subsurface electrical resistivity and chargeability data were qualitatively interpreted as spatial variations of pore-permeability and

water saturation indexes, related to lithological heterogeneities in the soil horizons described by the geotechnical data. To control the lateral water exudation, it was suggested to increase the number and dimensions of the lateral drains and to add a layer of compacted clay material bellow the garden soil. The overall results also indicated that certain underground structures, containing materials with highly contrasting electrical properties, can produce negative apparent resistivity values, contrary to the general perception that such results indicate noise or experimental errors.

ACKNOWLEDGMENTS

The authors would like to thank Capes for providing a scholarship to Jorge Luis Abril Benjumea for his Master degree. They also would like to thank the IG-CPGG/UFBA and EP/UFBA for providing the infrastructural and environmental support for this research.

REFERENCES

- Barbosa, J.S.F., Correa-Gomes, L.C., Dominguez, J. M. L., Cruz, S. A. S., Souza, J. S. D., 2005. Petrografia e litogeoquímica das rochas da parte oeste do Alto de Salvador, Bahia. *Revista Brasileira de Geociências*, São Paulo, 35(4): 9–22.
- Benjumea JL. 2018. Imageamento geométrico bidimensional como ferramenta na solução de problemas hidrológicos e geotécnicos na área urbana de Salvador, Bahia: Master Thesis, Universidade Federal da Bahia. Brazil. 70 pp.
- Bogoslovsky, V.A., Ogilvy, A.A., 1977. Geophysical methods for the investigation of landslides. *Geophysics*, 42: 562–571.
- Cosenza, R., Marmet, E., Rejiba, F., Cui, Y.J., Tabbagh, A., Charlery, Y., 2006. Correlations between geotechnical and electrical data: a case study at Garchy in France. *J. Appl. Geophys.* 60: 165–178.
- De Moraes, S., 2008. Diagnóstico hidrogeológico, hidrogeoquímico e da qualidade da Água do aquífero freático do alto cristalino de Salvador-Bahia: PhD Thesis, Universidade Federal da Bahia. Brazil. 214 pp.
- Friedel, S., Thielen, A., Springman, S.M., 2006. Investigation of a slope endangered by rainfall-induced landslides using 3D resistivity tomography and geotechnical testing. *J. Appl. Geophys.* 60: 100–114.
- Geotomo, 2010. RES2DINV ver. 3.59 For Windows XP/VISTA/7 - Rapid 2-D resistivity and IP inversions using the least square method. Manual. Geotomo Software, Penang, Malaysia.
- Godio, A., Bottino, G., 2001. Electrical and electromagnetic investigation for landslide characterization. *Phys. Chem. Earth (C)* 26: 705–710.
- Jung, H-K., Min, D-J., Oh, S., Chung, H., 2009. Negative apparent resistivity in dipole-dipole electrical survey. *Exploration Geophysics* 40: 33–40.
- Loke, M.H., Barker, R.D., 1996. Rapid least-squares inversion of apparent resistivity pseudo-sections using a quasi-Newton method. *Geophys. Prospect.* 44: 131–152.
- Oh, J-D., Jung, H-K., Min, D-J., 2011. Negative apparent resistivity based on physical modeling. *EGU General Assembly, Geophysical Research Abstracts* 13: 5435.
- Rudin, L. I., Osher, S., & Fatemi, E. 1992. Nonlinear total variation based noise removal algorithms. *Physica D: Nonlinear Phenomena*, 60(1-4): 259–268.
- Samouëlian, A., Cousin, I., Tabbagh, A., Bruand, A., Richard, G., 2005. Electrical resistivity survey in soil science: A review. *Soil & Tillage Research*, 83: 173–193.
- Sudha, K., Israil, M., Mittal, S., Rai, J., 2009. Soil characterization using electrical resistivity tomography and geotechnical investigation. *J. Appl. Geophys.* 67: 74–79.

J.L.A.B.: performed the processing and interpretation of geophysical data, and also contributed to writing the article; **O.A.L.L.:** contributed to write the article and to analyze the geophysical data; **L.E.C.:** contributed to analyze and interpret geotechnical data.

Received on March 20, 2021 / Accepted on October 26, 2021